Charge Transport of Hydrochloric Acid Doped Polyaniline and Poly(o-toluidine) Fibers: Role of Processing

ARTICLE *in* MACROMOLECULES · SEPTEMBER 1994

Impact Factor: 5.8 · DOI: 10.1021/ma00098a047

Charge Transport of Hydrochloric Acid Doped Polyaniline and Poly(*o*-toluidine) Fibers: Role of Processing

Y. Z. Wang and J. Joo

Department of Physics, The Ohio State University, Columbus, Ohio 43210-1106

C.-H. Hsu

Central Research and Development, Experimental Station, DuPont Company, Wilmington, Delaware 19880

J. P. Pouget

Laboratoire de Physique des Solides (CNRS URA 2), Université de Paris-Sud, 91405 Orsay, France

A. J. Epstein*

Departments of Physics and Chemistry, The Ohio State University, Columbus, Ohio 43210-1106

Received March 14, 1994; Revised Manuscript Received June 27, 1994®

ABSTRACT: We report the results of transport (temperature dependent dc conductivity, thermoelectric power, and microwave frequency conductivity, and dielectric constant) and structural studies for hydrochloric acid doped polyaniline (PAN-HCl) fibers 4-fold stretched at 300, 350, and 400 °C and the results of dc conductivity for its methyl ring-substituted derivative, poly(*o*-toluidine) (POT-HCl) fibers. For the PAN-HCl fibers, with increasing stretching temperatures, the system shows greater localization, as indicated by the decreasing conductivity with stronger temperature dependence and decreasing microwave dielectric constant with weaker temperature dependence. This is in accord with the observed decreasing crystallinity with increasing processing temperature. The interrupted metallic strands model is used to account for the microwave results assuming that the size of the metallic regions increases linearly with temperature. For the POT-HCl fiber, the conductivity is similar to that for the POT-HCl powder. When the fiber is stretched 3-fold, the conductivity increases almost 1 order of magnitude while the temperature dependence changes only slightly, in agreement with the short localization length in the system.

Introduction

Polyaniline consists of a large class of polymers which exist in three different discrete oxidation states at the molecular level: leucoemeraldine, emeraldine, and pernigraniline.[1,2] The polyaniline emeraldine base (PAN-EB) can be dissolved in *N*-methylpyrrolidinone (NMP)[3] or other organic solvents without changing the structure of the polymer backbone. As a consequence, high quality free standing films of PAN-EB can be cast from solution in NMP. Moreover, the as prepared films can be stretch-oriented at elevated temperatures (>110 °C, dependent on NMP content)[4] or by zone drawing at ~180 °C.[5,6] The insulating PAN-EB films subsequently can be doped with aqueous protonic acid such as HCl to form conducting emeraldine salts (PAN-ES), the conductivities of which are typically in the metallic regime for fully protonated samples. The hydrochloride salt form of polyaniline[7-9] and its methyl[10] and ethoxy[11] derivatives have been extensively studied. The samples studied are typically in the form of powder or film, with fibers and stretch oriented fibers being less frequently studied.[12,13] In this paper we report the results of transport (temperature dependent conductivity $\sigma_{dc}(T)$, thermoelectric power $S(T)$, and microwave frequency (6.5 GHz) conductivity $\sigma_{mw}(T)$, and dielectric constant $\epsilon_{mw}(T)$) and structural studies for the HCl doped polyaniline emeraldine fibers 4-fold stretched at 300 °C (PAN-HCl(300 °C)), 350 °C (PAN-HCl(350 °C)) and 400 °C (PAN-HCl(400 °C)). The dc conductivities for the HCl doped poly(*o*-toluidine) (POT-HCl), a methyl ring-substituted derivative of polyaniline, fibers (both as prepared and 3-fold stretched) are also reported.

® Abstract published in *Advance ACS Abstracts*, August 1, 1994.

Experimental Section

(a) Preparation of PAN Fiber. (1) Synthesis of PAN-EB, Spinning and Fiber Drawing. The synthesis of polyaniline in the emeraldine base oxidation state has been reported previously.[2] The inherent viscosity of the polymer was 1.31 (at 30 °C, as a 0.5 wt % solution in 96% H_2SO_4). The polymer was made into a solution and spun in the same manner as described in ref 13. The as-spun fiber was stretched 4-fold over a hot pin held at 300, 350, or 400 °C. The fiber drawing was carried out manually with 1 g (10^{-2} N) tension at an approximate rate of 10 cm/min.

(b) Preparation of Poly(2-methylaniline) (POT) Fiber. (1) Synthesis of POT. A solution of 154.5 g of 2-methylaniline, 194.4 g of 27 wt % HCl solution, and 1350 g of deionized water was placed into a 2 L jacketed glass reaction vessel under nitrogen atmosphere. The solution, kept at −8 °C, was stirred continuously. An oxidant solution of 155 g of ammonium persulfate dissolved in 270 g of water was added to the reaction medium at a rate of 1.95 mL/min. After stirring and cooling at −7 °C for 3.5 days, the solids formed were filtered off and washed repetitively with copious amount of water. The polymer was then converted to the base form by stirring the polymer powder with about 1–1.5 L of 0.15 M ammonium hydroxide solution for about 24 h, twice. The neutralized polymer was subsequently washed extensively with methanol and acetone and then dried to constant weight in a vacuum. The inherent viscosity of the polymer was 0.45 (at 30 °C, as a 0.5 wt % solution in 96% H_2SO_4), in contrast to 1.31 for PAN. The POT polymer was extremely soluble in methylene chloride and NMP. NMP was chosen as a solvent for spinning because it was found that the NMP solution was more extensible.

0024-9297/94/2227-5871$04.50/0

(2) POT/NMP Solution Preparation, Spinning and Fiber Drawing. A 33.2% poly(2-methylaniline)/NMP solution was prepared by adding 6.67 g of poly(2-methylaniline) to 13.43 g of NMP. The mixture was stirred vigorously with a spatula for 30 min to obtain a fluid mixture. There was no indication of a tendency of the mixture to gel. The mixture was then transferred to a twin cell equipped with a crossover plate for mixing. The mixture was then pushed back and forth through the crossover plate for 1 h at room temperature to obtain a homogeneous solution. During the mixing, the cycle time between the twin cell remained unchanged under a constant pressure, indicating that the solution also did not gel under shearing. The solution was spun by pumping it through a 325 mesh screen and a single hole (0.004 in. diameter, 0.016 in. length) spinneret, through a 0.25 in. gap into an 11 in. long bath of the tap water. The monofilament was wound up on a motor driven bobbin, stored in deionized water for 24 h, and then dried in air. The as-spun fiber was tested (1 in. gauge length) for tenacity/elongation/modulus (T/E/M) and found to be 0.8 gpd (gram per denier)/48%/18 gpd, respectively.

Fiber drawing was carried out as follows: A hot pin kept at 220 °C was placed between two motor driven bobbins. One end of the as-spun fiber on the feed roll set at 5.5 ft/min was guided over the hot pin and wound up on the takeup roll set at 16 ft/min. The ratio of the two motor speeds yielded a 3-fold stretched fiber. The drawn fiber had a T/E/M of 2.4 gpd/17%/40 gpd, respectively.

(c) Acid Doping and Measurement Techniques. The undoped PAN-EB and POT-EB fibers were immersed (without tension) in 1 M aqueous HCl solutions for at least 48 h. The doped fibers were then pumped under dynamic vacuum for approximately 2 days.

The four probe technique used for the $\sigma_{dc}(T)$ measurement,[7] the thermoelectric power technique,[7] and the "cavity perturbation" technique utilized for the microwave measurement[14] were previously described. The diameter of the fiber sample is typically less than 50 μm, which is smaller than the skin depth of the sample at 6.5 GHz. The X-ray diffraction measurement technique and analysis were also described earlier.[15]

Experimental Results (PAN-HCl)

Parts a–c of Figure 1 show the dc conductivity as a function of temperature for the PAN-HCl(300 °C), PAN-HCl(350 °C), and PAN-HCl(400 °C) fibers, plotted as log σ_{dc} vs T^{-1}, log σ_{dc} vs $T^{-1/2}$, and $\log(T^{1/2}\sigma_{dc})$ vs $T^{-1/4}$, respectively. As the stretching temperature is increased from 300 to 400 °C, $\sigma_{dc}(T)$ decreases and shows a stronger temperature dependence, indicating that the system moves further away from the metal–insulator boundary toward the insulating regime. On the insulating side of the metal–insulator transition, the conductivity generally can be described by

$$\sigma(T) = BT^{m} \exp[-(T_0/T)^{x}] \quad (1)$$

where B, m, T_0, and x are constants. Most known laws governing the conductivity are particular cases of eq 1. For example, $x = 1/4$ and $m = -1/2$ for the well-known three-dimensional Mott variable range hopping (VRH) law;[16] $x = 1/2$ and $m = 0$ for quasi-one-dimensional variable range hopping;[8,10] and $x = 1$ and $m = 0$ for Arrhenius-type activation. We analyze the activation energy T_0 and the exponent x below.

The $S(T)$ of fibers stretched at 300 and 350 °C are similar with $S(300\ K) \simeq +5\ \mu V/K$, decreasing linearly with decreasing T, with a slope of $\sim 4 \times 10^{-2}\ \mu V/K^2$, within the region of measurement ($240\ K < T < 300\ K$).

The microwave dielectric constant $\epsilon_{mw}(T)$ clearly distinguishes the different behaviors of the three fibers, Figure 2. For the PAN-HCl(300 °C) fiber, $\epsilon_{mw}(T)$ is high ($\sim$3000 at room temperature and $\sim$100 at $T \rightarrow 0$) and shows strong temperature dependence. In contrast, for the PAN-HCl(400 °C) fiber, $\epsilon_{mw}(T)$ is low ($\sim$20) and almost temperature independent. The $\epsilon_{mw}(T)$ for the PAN-HCl(350 °C) fiber is moderate ($\sim$120 at room temperature and $\sim$50 at $T \rightarrow 0$) with linear temperature dependence. The microwave conductivity $\sigma_{mw}(T)$ and the corresponding $\sigma_{dc}(T)$ of the PAN-HCl(350 °C) and PAN-HCl(400 °C) fibers are comparable at room temperature with increasing deviation as the temperature is lowered, typical for hopping transport in localized systems, Figure 3. For the PAN-HCl(300 °C) fiber, the situation is somewhat different. $\sigma_{mw}(T)$ is only weakly temperature dependent at high temperatures and decreases more rapidly below 140 K, the same temperature below which $\epsilon_{mw}(T)$ has a weaker quasi-linear T dependence.

The X-ray diffraction studies indicate a degradation of crystalline order for samples drawn at temperatures greater than 300 °C. The emeraldine base fiber stretched at 300 °C has a sizable crystallinity of about $X_c \sim 60 \pm 10\%$, similar to that for the stretched highly (physically) cross-linked emeraldine EB-II films reported earlier.[9,17] However, EB fibers stretched at 350 °C have only medium crystallinity with a larger amorphous content, while EB fibers stretched at 400 °C are amorphous with a slight orientation indicated in the X-ray pattern. Upon doping with 1 M HCl, the fiber stretched at 400 °C remains amorphous with a broad halo at d $\sim$ 4.2 Å exhibiting a slight orientation. The fiber stretched at 300 °C shows ES-II[15] crystalline order with well-defined (010) equatorial and (002) meridional reflections of d spacing 8.1 and 5.15 Å, respectively, and two broad equatorial (020) and (200) reflections of 4.1 and 3.6 Å, respectively. By applying the Scherrer formulas to the width of the two former reflections, interchain and intrachain crystalline domain sizes of $\epsilon_\perp \sim 60$ Å and $\epsilon_\parallel \sim 50$ Å, respectively, have been estimated. The percent crystallinity has been reduced with doping to about $X_c \sim 25 \pm 10\%$, and there is substantial paracrystalline disorder with the crystalline regions. The fiber stretched at 350 °C and subsequently doped is intermediate in order between those stretched at 300 and 400 °C. It exhibits only one X-ray diffraction peak, corresponding to an 8 Å interchain repeat distance (for a crystalline domain length $\xi_\perp$ of 40 Å), while the other reflections have merged into the broad amorphous halo.

Discussion (PAN-HCl)

Earlier studies by Joo *et al.*[9] have demonstrated the sensitivity of the microwave frequency dielectric constant to the degree of localization. We estimate the localization length, L, using

$$\epsilon_{mw}(T) = \epsilon_0 + (2^{9/2}/\pi^3)e^2N(E_F)L^2 \quad (2)$$

where ϵ_0 ($\sim$10) is from the estimated dielectric constant of the polymer backbone, e is the electron charge, and $N(E_F)$ ($\sim$1.6 states/eV-two rings[8] for the ES-II structure) is the density of states at the Fermi level. The results are shown in Table 1. The localization length at $T \rightarrow 0$, $L_\parallel(T \rightarrow 0)$, corresponds to the size of the region over which electrons are delocalized in the direction parallel to the stretched fiber. It is compared in Table 1 to the crystalline domain size, ξ, obtained from X-ray diffraction. It is clear from Table 1 that both the size of the crystalline regions and $L_\parallel(T \rightarrow 0)$ decrease significantly as the stretching temperature increases, in accord with the increasing disorder introduced with higher processing temperature. For each of the polymer fibers stretched at different temperatures, the conduction electron localization length

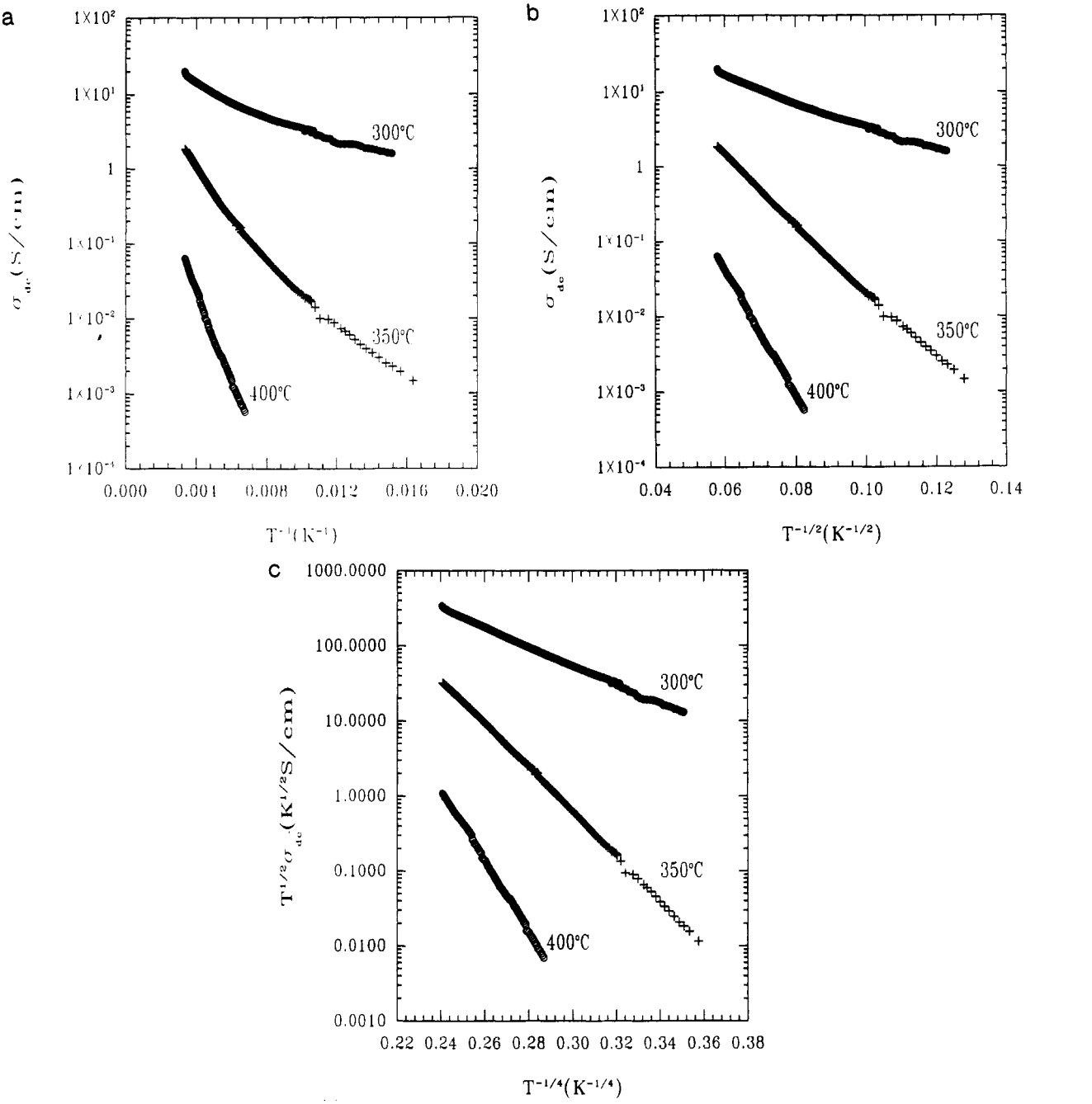

Figure 1. (a) $\sigma_{dc}(T)$ for PAN-HCl fibers 4-fold stretched at 300 °C (●), 350 °C (+), and 400 °C (○) as a function of T^{-1}. (b) $\sigma_{dc}(T)$ for PAN-HCl fibers 4-fold stretched at 300 °C (●), 350 °C (+), and 400 °C (○) as a function of $T^{-1/2}$. (c) $T^{1/2}\sigma_{dc}(T)$ for PAN-HCl fibers 4-fold stretched at 300 °C (●), 350 °C (+), and 400 °C (○) as a function of $T^{-1/4}$.

increases with increasing measurement temperature. This indicates the progressive delocalization of conduction electrons into the amorphous regions as the measurement temperature increases. In this regime, the charge transport can be understood using a modification of the interrupted metallic strands (IMS) model.[18]

The IMS model is based on linear metallic strands interrupted by insulating lattice defects. The interrupted metallic strands are modeled by metallic boxes with mean length L_0 which corresponds to the localization length of the charge carriers. The frequency (ω) dependent dielectric constant associated with the carrier motion is

$$\epsilon(\omega) = \frac{1 + \lambda\omega_P^2\tau_R^2}{(1 - i\omega\tau_R\lambda)(1 - i\omega\tau_R)} \tag{3}$$

Here ω_P is the carrier plasma frequency and $\lambda = \tau_0/(\tau_0 + \tau_R)$, where τ_R and τ_0 are the relaxation times for the metallic strands with and without defects, respectively. In the low temperature regime where $\tau_0 \gg \tau_R$, $\lambda \to 1$, and $\epsilon(\omega)$ becomes

$$\epsilon(\omega) = \frac{1 + \omega_P^2\tau_R^2}{(1 - i\omega\tau_R)^2} \tag{4}$$

In the microwave frequency range where $\omega\tau_R \ll 1$, the microwave dielectric constant can be simplified to

$$\epsilon_{mw} = 1 + \omega_P^2\tau_R^2 \tag{5}$$

τ_R is determined by the time it takes for a charge carrier to traverse a mean metallic box length, that is, $\tau_R \propto L$.

To first-order approximation, we assume that L increases linearly with measurement temperature, i.e.

$$L(T) = \xi + \alpha T \tag{6}$$

where ξ is the size of the "metallic islands" or the localization length at $T \to 0$, and α is a constant measuring the coupling strength between the metallic boxes. α is large for well coupled metallic boxes and small for poorly coupled ones. Assuming $\tau_R = L(T)/v_F$, where v_F is the Fermi velocity, we have

$$\tau_R = (\xi + \alpha T)/v_F \tag{7}$$

Substituting eq 7 into eq 5, we have

$$\epsilon_{mw} = 1 + \omega_p^2(\xi + \alpha T)^2/v_F^2 = \omega_P^2(\xi^2 + 2\alpha\xi T + \alpha^2 T^2)/v_F^2 \tag{8}$$

So for small α, ϵ_{mw} will show linear T dependence, while for large α it will be dominated by the T^2 term.

It is useful to apply this model to the observed ϵ_{mw} for fibers stretched at three different temperatures (given in parentheses). For the PAN-HCl(350 °C) fiber, $\epsilon_{mw}(T)$ is linearly proportional to the measurement temperature up to room temperature, suggesting the poor coupling (α small) between the "metallic islands". As a result, the charge carriers are localized to one or two "metallic islands". For the PAN-HCl(400 °C) fiber, the almost measurement temperature independent $\epsilon_{mw}(T)$ implies that $\alpha \simeq 0$. The coupling between the electronic states is so weak that the charge carriers are essentially localized even at high temperatures, consistent with the very strong temperature dependence of $\sigma_{dc}(T)$ (see below). For the PAN-HCl(300 °C) fiber, however, $\epsilon_{mw}(T)$ is linearly proportional to the measurement temperature only below ~140 K. Above this temperature, $\epsilon_{mw}(T)$ increases rapidly, suggesting the existence of strongly coupled metallic islands. The fact that $\epsilon_{mw}(T)$ can be represented by the sum of linear and higher order T terms ($\epsilon_{mw}(T) = A + BT + CT^2 + DT^3$ with A = 167.7, B = 0.942 K^{-1}, C = 0.000 138 K^{-2}, and D = 0.000 102 K^{-3}) indicates that the system is a mixture of better coupled and less well coupled metallic islands. The existence of the well coupled regions enables the charge carriers to be delocalized over several metallic islands at high measurement temperatures, in agreement with the estimated localization length (see Table 1).

By analyzing the reduced activation energy[19,20]

$$W(T) = d \ln \sigma(T)/d \ln T = \Delta E(T)/kT \tag{9}$$

where $\Delta E(T)$ is the effective activation energy, we are able to gain insight into the conduction mechanism through the amorphous portions separating the crystalline regions. Using eq 1,

$$W(T) = m + x(T_0/T)^x \tag{10}$$

For an activated $\sigma(T)$, m is typically much smaller than $x(T_0/T)^x$, thus

$$\log W(T) \simeq \log(xT_0^x) - x \log T \tag{11}$$

The value of x can be found from the slope of log $W(T)$ versus log T.

Figure 4 shows $W(T)$ as a function of measurement temperature on a double logarithmic scale for fibers drawn at the three different stretching temperatures. The value x can be found from the linear regions in Figure 4. For the PAN-HCl(400 °C) fiber, $x \simeq 0.40$. Using $x = 0.50$, $T_0 \simeq 3.7 \times 10^4$ K, similar to that reported earlier[8] for samples dominated by quasi-one-dimensional VRH in the disordered regions. For the PAN-HCl(350 °C) and PAN-HCl(300 °C) fibers, however, x is reduced to ~0.30 and ~0.25, respectively, suggesting the dominance of 3D VRH at low temperatures for these materials. By plotting $\ln(T^{1/2}\sigma_{dc})$ as a function of $T^{-1/4}$, we obtain $T_0 \simeq 2.3 \times 10^7$ K and 6.4 $\times 10^5$ K for the PAN-HCl(350 °C) and PAN-HCl(300 °C) fibers, respectively.

We compare the results for the fiber samples with those for films. For the PAN-HCl(300 °C) fiber, the low

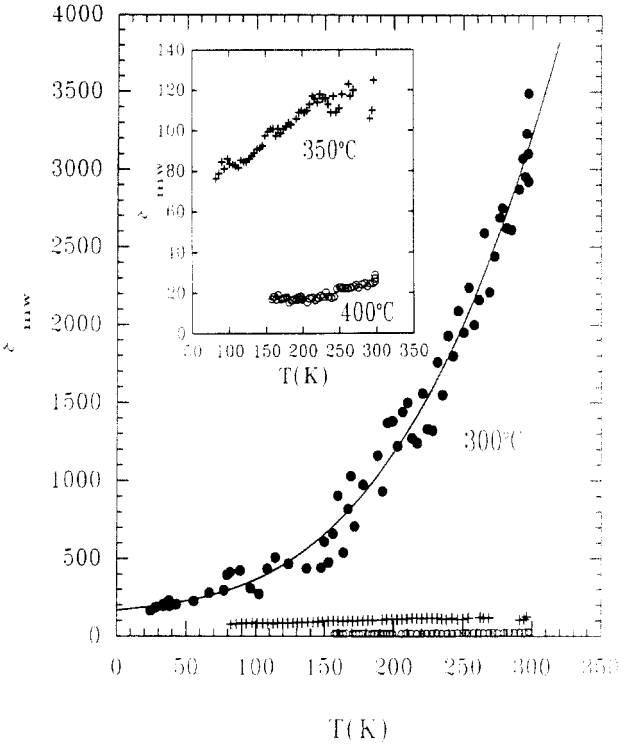

Figure 2. Temperature dependence of microwave dielectric constant $\epsilon_{mw}(T)$ for PAN-HCl fibers 4-fold stretched at 300 °C (●), 350 °C (+), and 400 °C (○). The solid line is the fit of $\epsilon_{mw}(T)$ of the 300 °C stretched sample to $\epsilon_{mw}(T) = A + BT + CT^2 + DT^3$ with A = 167.7, B = 0.942 K^{-1}, C = 0.000 138 K^{-2}, and D = 0.000 102 K^{-3}. Inset: ϵ_{mw} for the 350 and 400 °C samples on an expanded scale.

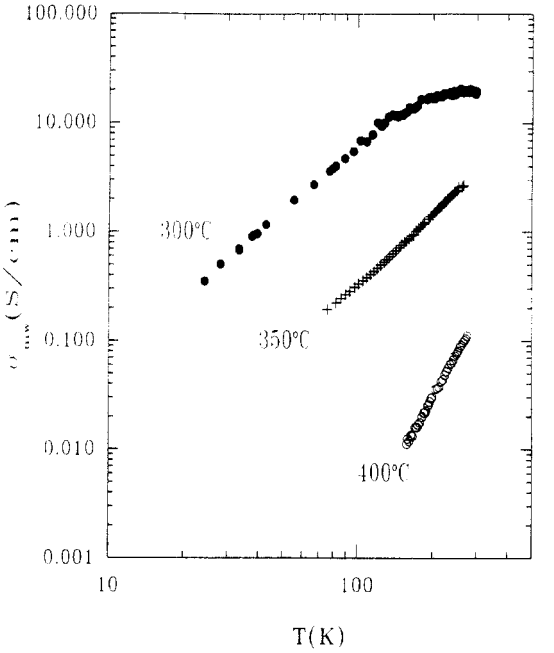

Figure 3. Temperature dependence of microwave conductivity $\sigma_{mw}(T)$ for PAN-HCl fibers 4-fold stretched at 300 °C (●), 350 °C (+), and 400 °C (○).

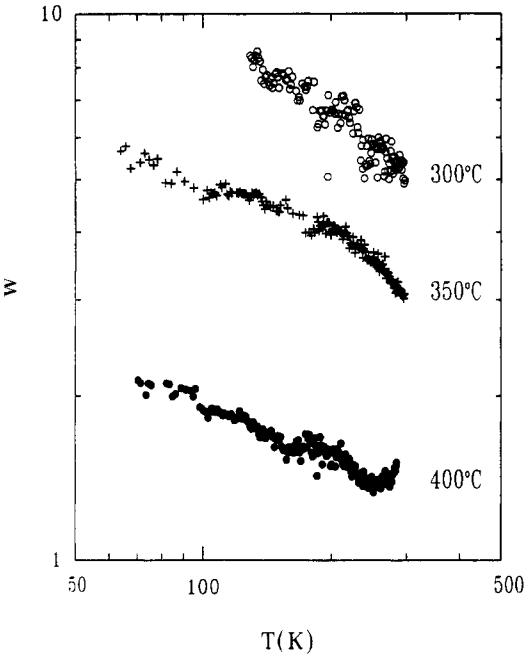

Figure 4. Temperature dependence of the reduced activation energy $W(T)$ for PAN-HCl fibers 4-fold stretched at 300 °C (●), 350 °C (+), and 400 °C (○).

Table 1. Crystalline Domain Size ξ Obtained from X-ray Diffraction and Localization Length $L_\parallel$ Determined from $\epsilon_{mw}(T)$ at $T \to 0$ and at Room Temperature for PAN-HCl Fibers

material	PAN-HCl (300 °C)	PAN-HCl (350 °C)	PAN-HCl (400 °C)
ξ(Å)	60 (⊥), 50 (∥)	40 (⊥)	~15
$L_\parallel(T \to 0)$ (Å)	50	30	12
$L_\parallel$(295 K) (Å)	230	45	14

temperature dielectric constant $\epsilon_{mw}(T \to 0)$ (~150) is ~50% larger than that for the PAN-HCl 4-fold stretched film reported by Wang *et al.*[8] ($\epsilon(T \to 0) \sim 100$), suggesting ~20% larger crystalline regions for the fiber sample, in accord with the X-ray results. In addition to the larger crystalline island size (especially in the perpendicular direction), X-ray structural studies show a somewhat smaller percent crystallinity for the fibers. Thus the metallic regions are likely further apart within the fiber. The large increase in ϵ_{mw} with increasing measurement temperature supports easy delocalization of charges from the crystalline into the adjacent disordered regions. The weaker temperature dependence of $\sigma_{dc}(T)$ for the PAN-HCl(300 °C) fiber reflects that the coupling between the metallic islands is stronger in the fiber sample. The smaller than expected σ_{dc} at room temperature for the PAN-HCl-(300 °C) fiber implies that not all the regions of the sample contribute to the dc conduction, a fraction of the sample being removed from the dc percolation path. As discussed above, the PAN-HCl(300 °C) fiber behaves as a mixture of well coupled and poorly coupled metallic islands, but the charge carriers will primarily follow the well coupled regions as the current path. The local order within parts of the primary conduction path through the disordered regions of the PAN-HCl(300 °C) fiber may favor three-dimensional VRH as opposed to the quasi-one-dimensional VRH typical for the oriented films. With increasing stretching temperature there is increasing disorder; the charge hopping through the disordered portions evolves toward the usual quasi-one-dimensional VRH ($\sigma_{dc}(T) \propto \exp[-(T_0/T)^{1/2}]$) for the 350 and 400 °C processed samples.

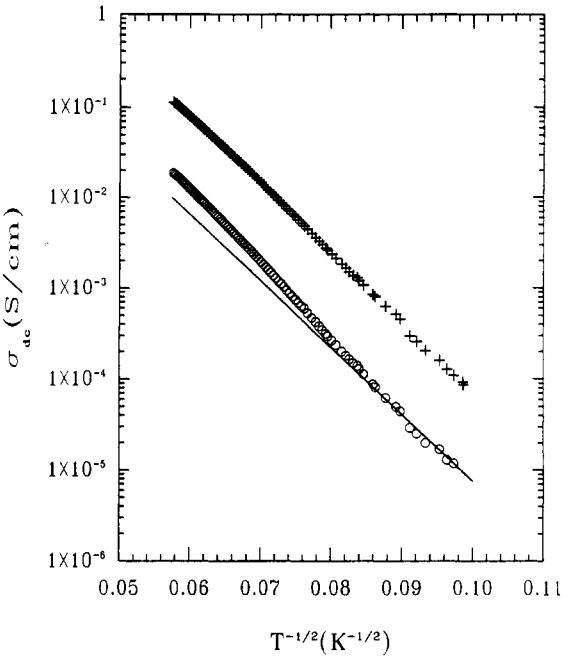

Figure 5. Temperature dependence of dc conductivity for POT-HCl fibers as prepared (○) and 3-fold stretched (+). The solid line is the conductivity for the POT-HCl powder from ref 10.

Experimental Results and Discussion (POT-HCl)

The behavior of the PAN-HCl fibers is in contrast to that of the methyl derivative, POT-HCl. Figure 5 shows the $\sigma_{dc}(T)$ for the POT-HCl fibers. For comparison, $\sigma_{dc}(T)$ for the POT-HCl powder from ref 10 is also shown (the solid line). The POT-EB fiber stretched 3-fold exhibits interchain broad reflections of spacing $d \sim 4.95$, 3.80, and 2.05 Å, close to that observed earlier for the POT-EB powder.[21] The stretched fiber is slightly more crystalline than the POT-EB powder.

With the substitution of a larger methyl group (CH_3) for one hydrogen atom on each benzene ring, more disorder is introduced into the POT-HCl system. This is reflected in the lower $\sigma_{dc}(T)$ with stronger temperature dependence, similar to that of the PAN-HCl(400 °C) fiber. The best fit for $\sigma_{dc}(T)$ is the quasi-one-dimensional VRH with $\sigma_{dc}(T) \propto \exp[-(T_0/T)^{1/2}]$. For the unstretched POT-HCl fiber, room temperature $\sigma_{dc}(T)$ is ~0.02 S/cm with $T_0 \simeq 3.8 \times 10^4$ K, similar to the results of the POT-HCl powder.[10] Upon stretching 3-fold, the room temperature $\sigma_{dc}(T)$ increases almost 1 order of magnitude while T_0 only decreases slightly to 3.2×10^4 K. The similar $\sigma_{dc}(T)$ between the POT-HCl fibers and powder demonstrates that for each of these POT-HCl systems electron localization caused by poor interchain coherence and increased interchain separation dominates.

Conclusion

As the processing temperature increases, the charge transport in 4-fold stretched PAN-HCl fibers shows the effects of greater localization due to increased disorder introduced into the system by higher temperature stretching. This is indicated by the measurement temperature dependent $\sigma_{dc}(T)$ and $\epsilon_{mw}(T)$ as well as the X-ray studies. The microwave behavior can be understood in the framework of the interrupted metallic strands model by assuming that the size of the metallic islands within individual fibers increases linearly with measurement temperature, with the largest effects in the samples stretched at lowest temperature and nearly negligent measurement temperature dependence in the samples

stretched at higher temperature. For the POT-HCl fibers, more disorder is introduced into the system by the substitution of a larger methyl group (CH_3) for one hydrogen atom on each benzene ring. The $\sigma_{dc}(T)$ for the unstretched POT-HCl fiber is similar to that of the POT-HCl powder, while that for the 3-fold stretched sample increases almost 1 order of magnitude though its dependence on measurement temperature changes only slightly.

Acknowledgment. The work was supported in part by the Office of Naval Research, NSF-INT Grant No. 90-16586, The OSU Center for Materials Research, and by an "Action Incitative" CNRS-NSF.

References and Notes

(1) MacDiarmid, A. G.; Epstein, A. J. *Conducting Polymers: Science and Technology*; Proceedings of the Second Brazillian Polymer Conference, Sao Paulo, Brazil, 5–8 Oct 1993; Plenum Publishing Corp.: New York, 1993; p 554.
(2) MacDiarmid, A. G.; Epstein, A. J. *Faraday Discuss. Chem. Soc.* **1989**, *88*, 317 and references therein.
(3) Angelopoulos, M.; Asturias, G. E.; Ermer, S. P.; Ray, A.; Scherr, E. M.; MacDiarmid, A. G.; Akhtar, M.; Kiss, Z.; Epstein, A. J. *Mol. Cryst. Liq. Cryst.* **1988**, *160*, 151.
(4) Cromack, K. R.; Jozefowicz, M. E.; Ginder, J. M.; Epstein, A. J.; McCall, R. P.; Du, G.; Leng, J. M.; Kim, K.; Li, C.; Wang, Z. H.; Druy, M. A.; Glatkowski, P. J.; Scherr, E. M.; MacDiarmid, A. G. *Macromolecules* **1991**, *24*, 4157.
(5) Kunugi, T.; Kawasumi, T.; Ito, T. *J. Appl. Polym. Sci.* **1990**, *40*, 2101.
(6) MacDiarmid, A. G.; Min, Y.; Wiesinger, J. M.; Oh, E. J.; Scherr, E. M.; Epstein, A. J. *Synth. Met.* **1993**, *55*, 753. Oh, E. J.; Wiesinger, J. M.; Manohar, S. K.; Scherr, E. M.; Prest, P. J.; MacDiarmid, A. G.; Epstein, A. J. *Synth. Met.* **1993**, *55*, 977.
(7) Zuo, F.; Angelopoulos, A.; MacDiarmid, A. G.; Epstein, A. J. *Phys. Rev. B* **1987**, *36*, 3475. Epstein, A. J.; Ginder, J. M.; Zuo, F.; Bigelow, R. W.; Woo, H.-S.; Tanner, D. B.; Richter, A. F.; Huang, W.-S.; MacDiarmid, A. G. *Synth. Met.* **1987**, *18*, 303.
(8) Wang, Z. H.; Li, C.; Scherr, E. M.; MacDiarmid, A. G.; Epstein, A. J. *Phys. Rev. Lett.* **1991**, *66*, 1745. Wang, Z. H.; Scherr, E. M.; MacDiarmid, A. G.; Epstein, A. J. *Phys. Rev. B* **1992**, *45*, 4190.
(9) Joo, J.; Oblakowski, Z.; Du, G.; Pouget, J. P.; Oh, E. J.; Wiesinger, J. M.; Min, Y.; MacDiarmid, A. G.; Epstein, A. J. *Phys. Rev. B* **1994**, *49*, 2977.
(10) Wang, Z, H.; Ray, A.; MacDiarmid, A. G.; Epstein, A. J. *Phys. Rev. B* **1991**, *43*, 4373. Wang, Z. H.; Javadi, H. H.; Ray, A.; MacDiarmid, A. G.; Epstein, A. J. *Phys. Rev. B* **1990**, *42*, 5411.
(11) Pouget, J. P.; Zhao, S. L.; Wang, Z. H.; Oblakowski, Z.; Epstein, A. J.; Manohar, S. K.; Wiesinger, J. M.; MacDiadmid, A. G.; Hsu, C.-H. *Synth. Met.* **1993**, *55–57*, 341.
(12) Tang, X.; Scherr, E. M.; MacDiarmid, A. G.; Epstein, A. J. *Bull. Am. Phys. Soc.* **1989**, *34*, 583.
(13) Hsu, C.-H.; Cohen, J. D.; Tietz, R. F. *Synth. Met.* **1993**, *59*, 37.
(14) Javadi, H. H.; Cromack, K. R.; MacDiarmid, A. G.; Epstein, A. J. *Phys. Rev. B* **1989**, *39*, 3579.
(15) Pouget, J. P.; Jozefowicz, M. E.; Epstein, A. J.; Tang, X.; MacDiarmid, A. G. *Macromolecules* **1991**, *24*, 779.
(16) Mott, N. M.; Davis, E. *Electronic Processes in Non-crystalline Materials*; Clarendon Press: Oxford, U.K., 1979.
(17) Pouget, J. P.; Oblakowski, Z.; Nogami, Y.; Albouy, P. A.; Laridjani, M.; Oh, E. J.; Min, Y.; MacDiarmid, A. G.; Tsukamoto, J.; Ishiguro, T.; Epstein, A. J. *Synth. Met.* **1994**, *65*, 131.
(18) Rice, M. J.; Bernasconi, J. *J. Phys. F: Metal Phys.* **1972**, *2*, 905.
(19) Zabrodskii, A. G.; Zinoveva, K. N. *Zh. Eksp. Teor. Fiz.* **1984**, *86*, 727; *Sov. Phys. JETP* **1984**, *59*, 425.
(20) Zabrodskii, A. G. *Fiz. Tekh. Poluprovodn.* **1980**, *14*, 1130; *Sov. Phys. Semicon.* **1980**, *14*, 670.
(21) Jozefowicz, M. E.; Epstein, A. J.; Pouget, J. P.; Masters, J. G.; Ray, A.; MacDiarmid, A. G. *Macromolecules* **1991**, *24*, 5863.